minerals

MDPI

Article

A Comparison Study on the Recovery of REEs from Red Mud by Sulfation Roasting–Water Leaching and Citric Acid Leaching

Hossein Shalchian [1,2,*], Mohsen Hajizadeh Navakh [1], Ionela Birloaga [2], Abolfazl Babakhani [1] and Francesco Vegliò [2,*]

[1] Department of Materials Science and Engineering, Engineering Faculty, Ferdowsi University of Mashhad, Mashhad 9177948974, Iran; babakhani@um.ac.ir (A.B.)
[2] Department of Industrial and Information Engineering and Economics (DIIIE), Engineering Headquarters of Roio, University of L'Aquila, 67100 L'Aquila, Italy; ionelapoenita.birloaga@univaq.it
* Correspondence: hossein.shalchian@univaq.it (H.S.); francesco.veglio@univaq.it (F.V.)

Abstract: In this study, the recovery of rare earth elements (REEs) from red mud (bauxite residue) was explored through a combination of citric acid leaching and sulfation roasting–water leaching processes, introducing an innovative approach to the field. The research uniquely investigates the influence of citric acid on the leaching behavior of REEs and impurities in both untreated red mud and red mud subjected to sulfation roasting, providing a direct comparison of these methodologies. A novel aspect of this study is the evaluation of solvent extraction efficiency using DEHPA, highlighting the selective recovery of REEs over impurities from both citric acid and water-leaching solutions. Furthermore, a comprehensive phase analysis using X-ray diffraction (XRD) was conducted to track the transformations of minerals during the sulfation roasting process, an original contribution to the literature. The findings revealed that over 85% of REEs and major elements such as Fe, Al, Ca, and Ti dissolved in water after sulfation at 105 °C, while iron and titanium dissolution significantly decreased following roasting at 725 °C. Importantly, terbium, neodymium, and gadolinium extraction efficiencies were notably affected by roasting temperature. Citric acid leaching results demonstrated that the direct leaching of red mud leads to higher leaching efficiency than leaching it after the roasting process. Solvent extraction demonstrated lower terbium and neodymium recovery from citric acid solutions compared to water leaching solution. Finally, stripping experiments illustrated that 6M H_2SO_4 solution is capable of stripping more than 80% of rare earth elements, except terbium.

Keywords: red mud; rare earth elements; sulfation–roasting; citric acid; leaching; solvent extraction

Citation: Shalchian, H.; Hajizadeh Navakh, M.; Birloaga, I.; Babakhani, A.; Vegliò, F. A Comparison Study on the Recovery of REEs from Red Mud by Sulfation Roasting–Water Leaching and Citric Acid Leaching. *Minerals* **2024**, *14*, 1044. https://doi.org/10.3390/min14101044

Academic Editors: Weslei Monteiro Ambros and Irineu Antonio Schadach Brum

Received: 9 September 2024
Revised: 6 October 2024
Accepted: 14 October 2024
Published: 18 October 2024

1. Introduction

Red mud is the by-product of the alkaline refining process of alumina, which is called the Bayer process. The application of pressure leaching on bauxite ore in an alkaline media leads to the dissolution of aluminum, leaving behind a reddish solid residue enriched with ferric oxide [1–3]. Nearly 2–3 tons of bauxite is consumed for the production of 1 ton of aluminum hydroxide in alumina refining factories, which leads to the generation of about 1–2.5 tons of red mud [4–6]. Considering the annual world production of aluminum, global alumina production systems discharged 200 million tons of red mud in 2021 [7]. Due to its high discharge rate and alkalinity, it is usually stored in dams and occupies large areas of land, inducing serious potential hazards to the environment [8]. According to statistics, currently more than 4.6 billion tons of red mud are estimated to be accumulated in global stockpiles [9]. Some physicochemical characteristics, such as its complex composition, large specific surface area, and strong alkalinity, pose challenges in finding large-scale applications for red mud [3,10]. On the other hand, red mud contains valuable components such as Al, Fe, Ti and rare earth elements (REEs) which are important from an economic point of view and for sustainable development, considering the scarcity and depletion of primary

resources [11]. Hence, it is necessary to develop efficient and economical technologies to consume large amounts of red mud effectively and overcome the environmental problems of its disposal [12].

There are two strategies in this regard. The first focuses on utilizing red mud as a consumable raw material in other sectors, based on its physicochemical properties. Its small particle size and porous structure provide a high specific surface area, making it a suitable candidate for use as an adsorbent and ion exchange material. Accordingly, it has found some applications in wastewater treatment [13–16] and waste gas treatment [17–19]. In addition, red mud contains oxides such as Fe_2O_3, SiO_2, Al_2O_3, CaO, and TiO_2, which makes it suitable for application in construction materials such as brick, cement, and concrete production [20–22], as well as in glass and ceramics [23,24] and catalysts [25–28].

The second strategy involves recovering valuable elements from red mud using hydrometallurgical and pyrometallurgical processes, or a combination of both methods [29]. In this regard, some researchers have focused on the recovery of iron [4,30–32], aluminum [33–35], or titanium [36–38], while other studies have considered REEs as valuable elements [39–44]. The total concentration of REEs in red mud is different and depends on the origin of the bauxite ore, but typically lies between 0.02% and 0.27% [1]. Considering the low concentration of REEs in comparison to the high values of other elements such as iron and aluminum, the selective extraction of REEs is a challenging issue.

The primary methods used in the metallurgical extraction of REEs from red mud are pyrometallurgy, hydrometallurgy, and biohydrometallurgy processes. Pyrometallurgical processes often come with high capital costs, require substantial energy, and contradict the goal of reducing the carbon footprint of value recovery from red mud. In contrast, hydrometallurgical processes offer several advantages, including lower capital costs, flexibility in processing complex secondary resources, the potential for diverse by-product recovery, relatively low energy consumption, and the ability to handle extremely low-grade materials [45].

Among the various hydrometallurgical methods applied for leaching using different acids [46], as well as for separation techniques like solvent extraction [47–50] and ion exchange [51,52], the combination of sulfation roasting pretreatment followed by water leaching [43] appears to be particularly attractive. This approach offers a high leaching rate of REEs, high selectivity, and the added benefit of sulfuric acid regeneration. In the direct acid leaching method, the high concentration of dissolved iron in the leach solution creates challenges for the subsequent recovery of REEs. However, during the sulfation process, the resulting sulfate salts of iron, aluminum, and titanium are converted into their corresponding water-insoluble oxides in the subsequent roasting stage. In contrast, REEs remain as soluble sulfates, which can be easily dissolved during the following water leaching step. This process results in the separation of the insoluble oxides of iron, aluminum, and titanium, leading to a high selectivity for REEs over impurities [43].

On the other hand, it has been demonstrated that carboxylic acids, such as citric acid, can selectively dissolve REEs from coal ash, leaving behind iron and aluminum impurities [53]. However, citric acid has rarely been used to dissolve REEs from red mud. One study showed that using citric acid resulted in lower leaching efficiency for iron compared to inorganic acids, indicating higher selectivity for REE dissolution from red mud [46]. The advantage of using citric acid as a leaching agent lies in its biodegradability, making it an environmentally friendly option for sustainable wastewater treatment. Therefore, further investigations are needed to explore its potential as a promising lixiviant for treating red mud.

Considering these advantages, this study aimed to investigate the effect of citric acid on the leaching behavior of REEs and impurities in a provided red mud sample. The study also explored the effect of citric acid on the leaching efficiency of REEs and impurities after sulfation roasting, comparing the results with the sulfation roasting–water leaching method. Subsequently, solvent extraction studies were conducted to evaluate the selective recovery of REEs over impurities across the methods used. This investigation, along with

the comparison between the employed methods, citric acid leaching and sulfation roasting–water leaching, followed by solvent extraction, is considered original in the context of existing studies, as reported in this paper. Additionally, a comprehensive phase study using XRD was conducted to examine the phase changes of different elements during the sulfation roasting process, which, to the best of our knowledge, is unprecedented in the literature.

2. Materials and Methods

2.1. Materials

A dried sample of agglomerated red mud was supplied by the Iran Alumina Company in northeast Iran. Preliminary milling was conducted to produce a homogeneous fine powder before further treatment. The moisture content of the sample was measured at approximately 0.9% after drying at 105 °C. X-ray fluorescence (XRF) and X-ray diffraction (XRD) methods were used to identify the major components of the homogeneous powder. The XRF analysis of the red mud sample is presented in Table 1. The rare earth element (REE) content was determined by chemical digestion using aqua regia, followed by ICP measurement, as shown in Table 2. The particle size distribution of the red mud was measured by a particle size analyzer (Figure 1). Analytical-grade sulfuric acid (VWR chemicals) and citric acid (Sigma-Aldrich, Wien, Austria) were used for the acid baking and leaching experiments.

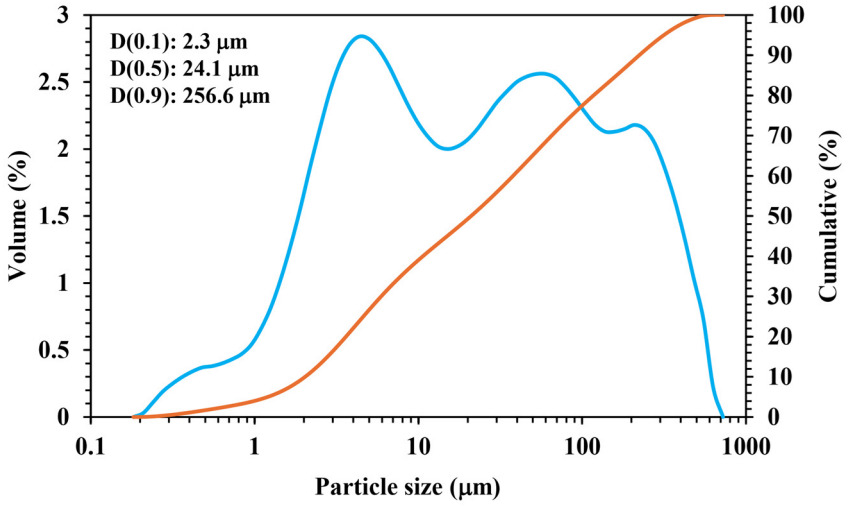

Figure 1. Particle size distribution and cumulative percentage of the red mud.

Table 1. Chemical composition of red mud determined by XRF.

Compound	Value (wt.%)
Fe_2O_3	24.63
CaO	19.04
SiO_2	15.36
Al_2O_3	14.69
TiO_2	4.69
Na_2O	3.92
MgO	1.12
K_2O	0.44
P_2O_5	0.11
MnO	0.07
SO_3	0.40
LOI	15.25

Table 2. Chemical composition of red mud determined by ICP-OES.

Rare Earth Element	Value (g/t)	Undesired Elements	Value (wt.%)
Y	45	Fe	18.47
Eu	4.3	Ca	13.76
Tb	22.9	Al	7.89
Dy	11.8	Ti	5.65
Nd	447		
La	93.9		
Ce	265		
Gd	42.2		

2.2. Acid-Baking Sulfation

In these experiments, varying amounts of sulfuric acid were added to red mud to create a homogeneous paste. The weight ratio of sulfuric acid to solid powder ranged from 0.5 to 2. A small amount of water was added during mixing to ensure proper homogenization. The mixture turned gray, and the temperature increased immediately as the sulfation reactions began. The homogenized pastes were then baked at 105 °C for 24 h. Finally, phase identification of the sulfated samples was carried out using XRD analysis.

2.3. Roasting

The goal of the roasting process is to convert sulfates into oxides. To achieve this, the baked samples from the sulfation reactions were roasted at 675 °C and 725 °C for two hours. The samples were first placed in a muffle furnace at room temperature and then heated up to the target temperatures. After two hours, the roasted samples were allowed to cool to ambient temperature and were subsequently analyzed by XRD.

2.4. Leaching

Leaching experiments were conducted in two groups. The first group involved simple water leaching at room temperature. Sulfated samples, both after acid baking and those roasted at 675 °C and 725 °C, were subjected to water leaching for 1 h with a pulp density of 2% wt./v. The second group focused on citric acid leaching at an elevated temperature. Initial red mud and roasted samples were leached in 0.5 M citric acid at 80 °C for up to 6 h with a pulp density of 5% wt./v. All experiments were carried out in a borosilicate glass reactor at a fixed temperature with magnetic stirring (1000 rpm). Solid–liquid phase separation was achieved using a vacuum filter with a 0.45 μm pore size. Finally, all solutions were analyzed by ICP.

2.5. Solvent Extraction Experiments

These experiments were conducted at room temperature, using DEHPA as the extractant and n-Heptane as the diluent. The organic/aqueous ratio and mixing speed were kept constant across all experiments. The effects of mixing duration and the extractant/diluent ratio were investigated. Sulfuric acid was used as the stripping agent, and the effect of acid concentration on the stripping process was also examined.

2.6. Characterization

X-ray fluorescence spectroscopy of the initial red mud was conducted using a Philips PW1480 instrument. The phase identification of all solid samples, including the initial red mud, sulfated samples under various conditions, and roasted samples, was performed using an XRD instrument (Explorer: G.N.R. srl, Agrate Conturbia, Italy). The particle size distribution of the red mud was measured by a Mastersizer 2000 (Malvern Instruments Ltd., Malvern, UK). The thermal analyses were carried out with a LINSEIS instrument, heating at a rate of 10 °C/min from ambient temperature to 1050 °C. The metal concentration measurements for all solutions were conducted using an ICP-OES (Agilent Technologies

5100, Santa Clara, CA, USA). It should be noted that all experiments were performed with a single repetition.

3. Results and Discussion

3.1. Thermodynamic Evaluations

The goal of the sulfation process is to convert metal oxides into their sulfate salts. According to the literature, most oxides in red mud can be converted to sulfates through acid mixing and drying [43]. By analyzing the variation in Gibbs free energy for sulfation reactions, the feasibility of these reactions for the desired elements can be assessed (Figure 2a). The probable sulfation reactions for the main impurities and REE oxides are as follows:

$$CaO + H_2SO_4 \rightarrow CaSO_4 + H_2O \quad (1)$$

$$Fe_2O_3 + 3H_2SO_4 \rightarrow Fe_2(SO_4)_3 + 3H_2O \quad (2)$$

$$Al_2O_3 + 3H_2SO_4 \rightarrow Al_2(SO_4)_3 + 3H_2O \quad (3)$$

$$TiO_2 + H_2SO_4 \rightarrow Ti(SO_4)O + H_2O \quad (4)$$

$$Y_2O_3 + 3H_2SO_4 \rightarrow Y_2(SO_4)_3 + 3H_2O \quad (5)$$

$$Eu_2O_3 + 3H_2SO_4 \rightarrow Eu_2(SO_4)_3 + 3H_2O \quad (6)$$

$$Tb_2O_3 + 3H_2SO_4 \rightarrow Tb_2(SO_4)_3 + 3H_2O \quad (7)$$

$$Dy_2O_3 + 3H_2SO_4 \rightarrow Dy_2(SO_4)_3 + 3H_2O \quad (8)$$

$$Nd_2O_3 + 3H_2SO_4 \rightarrow Nd_2(SO_4)_3 + 3H_2O \quad (9)$$

$$La_2O_3 + 3H_2SO_4 \rightarrow La_2(SO_4)_3 + 3H_2O \quad (10)$$

$$Ce_2O_3 + 3H_2SO_4 \rightarrow Ce_2(SO_4)_3 + 3H_2O \quad (11)$$

$$Gd_2O_3 + 3H_2SO_4 \rightarrow Gd_2(SO_4)_3 + 3H_2O \quad (12)$$

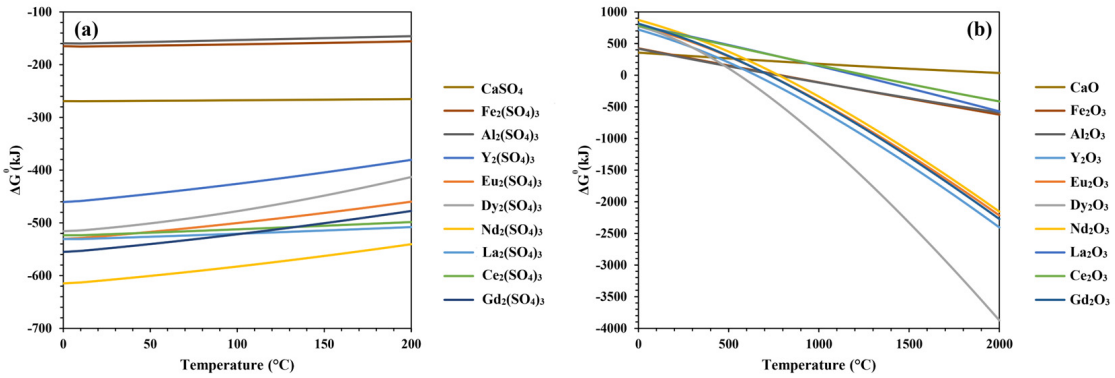

Figure 2. (**a**) Variation in the standard Gibbs free energy versus temperature for sulfation reactions, (**b**) Variation in the standard Gibbs free energy versus temperature for thermal decomposition of sulfates to oxides.

Variations in the standard Gibbs free energy, with temperature for the reactions described, were calculated using HSC Chemistry 6.0 software, and the results are presented in Figure 2a. These results clearly indicate that the ΔG° values for sulfation reactions are negative for the most significant impurities and REEs in red mud. Consequently, the sulfation reaction is theoretically feasible for all the elements mentioned. This suggests that most oxides in red mud can be easily converted to their respective sulfates through a simple acid-baking sulfation process.

Choosing an appropriate temperature is crucial from an economic standpoint. As shown in Figure 2a, ΔG° values remain negative across the entire temperature range, even

at ambient temperature. Therefore, the mixed samples were baked at 105 °C for 24 h to ensure sufficient time for the reactions to occur.

In general, the decomposition temperatures of REE sulfates are higher compared to those of main group or transition metal sulfates [54,55]. To achieve selective dissolution of rare earth elements over base metals, a subsequent roasting step was performed after the sulfation reaction. This step is necessary because REE sulfates are more stable than base metal sulfates within the applied temperature range. As a result, selective separation of water-soluble REE sulfates from undesirable base metal oxides can be achieved through simple water leaching.

Probable roasting reactions for sulfate-to-oxide conversion of the elements of interest are as follows:

$$CaSO_4 \rightarrow CaO + SO_3 \quad (13)$$

$$Fe_2(SO_4)_3 \rightarrow Fe_2O_3 + 3SO_3 \quad (14)$$

$$Al_2(SO_4)_3 \rightarrow Al_2O_3 + 3SO_3 \quad (15)$$

$$Ti(SO_4)O \rightarrow TiO_2 + SO_3 \quad (16)$$

$$Y_2(SO_4)_3 \rightarrow Y_2O_3 + 3SO_3 \quad (17)$$

$$Eu_2(SO_4)_3 \rightarrow Eu_2O_3 + 3SO_3 \quad (18)$$

$$Tb_2(SO_4)_3 \rightarrow Tb_2O_3 + 3SO_3 \quad (19)$$

$$Dy_2(SO_4)_3 \rightarrow Dy_2O_3 + 3SO_3 \quad (20)$$

$$Nd_2(SO_4)_3 \rightarrow Nd_2O_3 + 3SO_3 \quad (21)$$

$$La_2(SO_4)_3 \rightarrow La_2O_3 + 3SO_3 \quad (22)$$

$$Ce_2(SO_4)_3 \rightarrow Ce_2O_3 + 3SO_3 \quad (23)$$

$$Gd_2(SO_4)_3 \rightarrow Gd_2O_3 + 3SO_3 \quad (24)$$

Figure 2b illustrates the variation in standard Gibbs free energy versus temperature for the roasting reactions, as calculated by HSC Chemistry 6.0 software. The thermal decomposition of sulfates theoretically begins at temperatures where the plots intersect the $\Delta G = 0$ line. According to Figure 2b, calcium sulfate is the most stable compound, followed by cerium and lanthanum sulfates, with thermal decomposition temperatures exceeding 1000 °C. The remaining elements decompose at temperatures below 800 °C. The theoretical decomposition temperatures for the sulfates of interest are listed in Table 3.

Table 3. Theoretical and experimental thermal decomposition temperatures of sulfates for impurities and of REE in red mud.

Compound	Theoretical Decomposition Temperatures (°C)	Experimental (Onset) Decomposition Temperatures (°C)	Heating Rate (°C/Min)	Reference
$CaSO_4$	2280	>1000	-	[56]
$Fe_2(SO_4)_3$	784	545	5	[54]
$Al_2(SO_4)_3$	769	524	5	[54]
$Ti(SO_4)O$	-	430	-	[56]
$Y_2(SO_4)_3$	650	850	2.5	[43]
$Eu_2(SO_4)_3$	726	810	3	[57]
$Tb_2(SO_4)_3$	-	820	10	[58]
$Dy_2(SO_4)_3$	559	-	-	-
$Nd_2(SO_4)_3$	778	800	1.5	[43]
$La_2(SO_4)_3$	1209	840	2.5	[43]
$Ce_2(SO_4)_3$	1262	666	5	[54]
$Gd_2(SO_4)_3$	725	1001	10	[59]

The data in Table 3 show that the thermal decomposition temperatures of undesirable elements like iron and aluminum are very close to those of REEs. However, experimental results reported in the literature differ from the theoretical temperatures calculated in this study. As indicated in the third column of Table 3, iron, aluminum, and titanium sulfates begin to decompose at temperatures below 600 °C, while the decomposition temperatures for REEs are higher than 600 °C. Therefore, it is possible to perform roasting at an appropriate temperature that converts the sulfates of impurities into their oxides, while keeping the REE sulfates stable.

3.2. Phase Identification of Red Mud

Figure 3a shows that calcium is predominantly present in the structures of Calcite, Hydrogarnet, and Laumontite. As expected, the main iron phase in the red mud sample is Hematite. Aluminum is found in the structures of Hydrogarnet, Cancristilite, and Laumontite, with Cancristilite and Laumontite being silicate compounds.

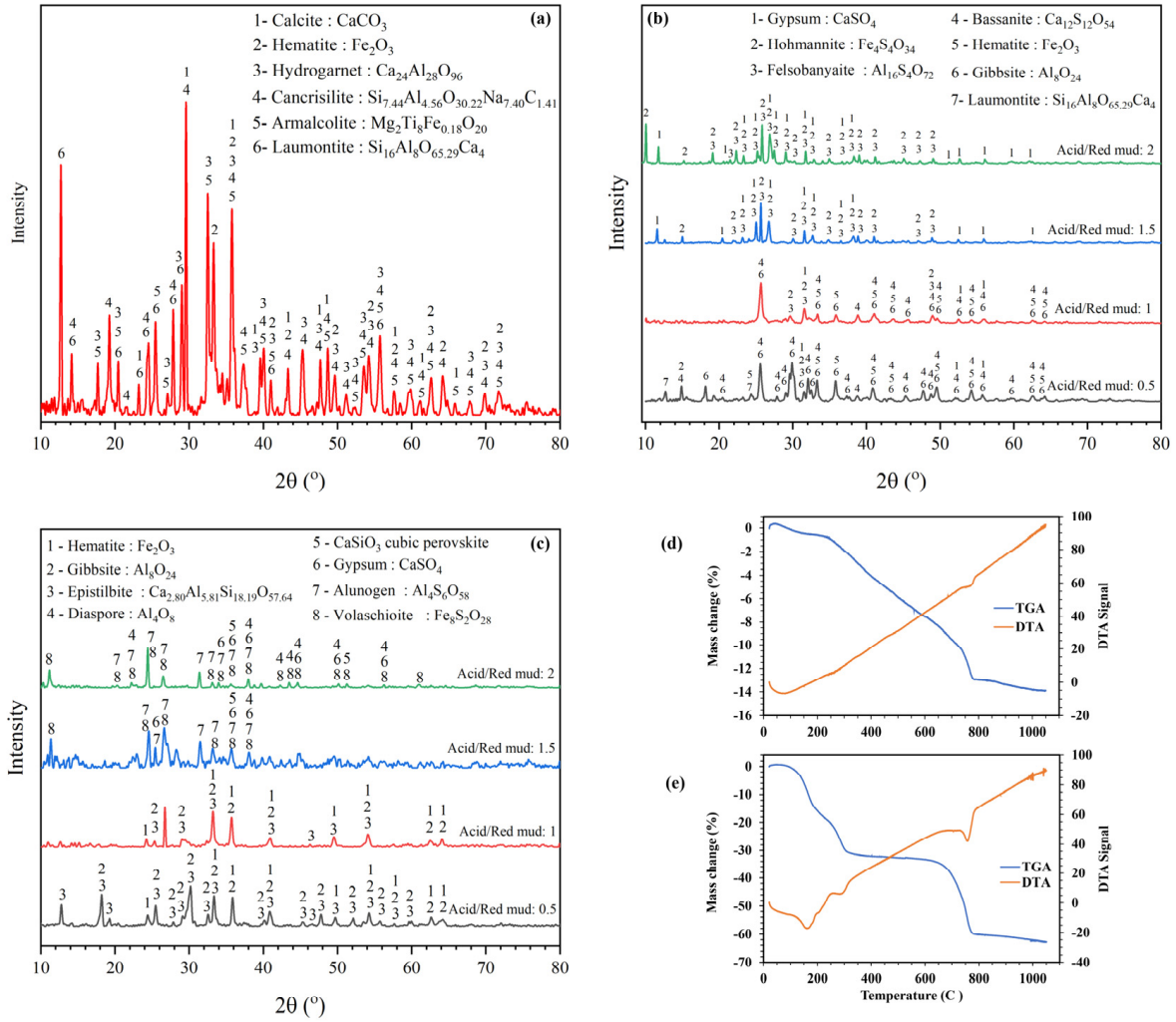

Figure 3. (**a**) XRD pattern of red mud, (**b**) XRD patterns of sulfated samples at different acid/red mud weight ratios, (**c**) XRD patterns of filter cake after water leaching of sulfated samples at different acid/red mud weight ratios, (**d**) TGA-DTA graphs for red mud and (**e**) TGA-DTA graphs for sulfated sample, at heating rate of 10 °C/min.

According to the XRF analysis (Table 1), titanium and magnesium are also present in notable amounts, rather than as mere traces. These elements, along with some iron, are observed in the composition of Armalcolite. Silicon is primarily found in the silicate compounds Cancristilite and Laumontite.

3.3. Phase Analysis of the Sulfated Samples

The XRD patterns of the sulfated samples at different acid/red mud weight ratios are presented in Figure 3b. It is evident that some oxide phases of Al and Fe persist in sulfated samples with lower acid/red mud weight ratios of 0.5 and 1. At the lowest ratio of 0.5, aluminum is mainly present as Gibbsite (an oxide) and Laumontite (a silicate compound) alongside calcium. It appears that aluminum-containing phases such as Hydrogarnet and Cancristilite in the primary red mud are converted to Bassanite and Gibbsite at this acid/red mud weight ratio. Laumontite also began to dissociate, though the reaction was not complete. Increasing the acid to a ratio of 1 led to the complete dissociation of Laumontite and the formation of an aluminum oxide sulfate phase known as Felsobanyatite. The intensity of Gibbsite peaks decreased, indicating that primary aluminum compounds in red mud are more fully converted to sulfates rather than oxides at this acid concentration. Figure 3b also shows that with higher acid ratios of 1.5 and 2, there are no traces of oxide and silicate compounds such as Gibbsite and Laumontite, demonstrating the complete conversion of aluminum into the oxide sulfate phase of Felsobanyatite. Water leaching experiments discussed in the following sections confirm that this aluminum oxide sulfate is mostly soluble in water.

Regarding iron, the ratio of 0.5 is insufficient for complete sulfation. Hematite remains the dominant iron phase at this ratio (Figure 3b). At a ratio of 1, increased acid concentration reduces the intensity of Hematite peaks and increases the intensity of Hohmannite, an iron oxide sulfate. With an acid ratio of 1.5, Hematite peaks disappear completely, leaving only the Hohmannite phase detectable. It is important to note that Hohmannite is not a pure sulfate phase; it contains more oxygen than a stoichiometric sulfate, making it an oxide sulfate compound that is also nearly soluble in water, as indicated by subsequent results.

For calcium, only small peaks of Gypsum and Bassanite were observed at acid/red mud weight ratios of 0.5 and 1. As the acid ratio increased to 1.5 and 2, Bassanite disappeared, and all calcium converted to Gypsum. Bassanite, an oxide sulfate compound, was completely converted to Gypsum with increasing acid concentration (Figure 3b).

Based on the XRD patterns in Figure 2a,b, the Armalcolite phase in red mud also decomposed, but no traces of resulting compounds containing silicon and titanium were detected. This is likely due to the decomposition of Armalcolite into trace amounts of partial compounds that were not detectable by XRD in this investigation.

3.4. Phase Analysis of Water-Insoluble Compounds in the Sulfated Samples

Phase analysis of different sulfated samples was performed in the previous section. To assess the amount of insoluble compounds and evaluate the effectiveness of the sulfation process, samples with varying acid additions were dissolved in water.

The water-insoluble compounds were collected as solid residues. The weight loss measured during leaching indicates the amount of water-insoluble compounds. Table 4 presents the weight loss results during water leaching for different sulfated samples. The highest weight loss, at 97.73%, was observed in the sulfated sample with an acid/red mud weight ratio of 2.

Table 4. Weight loss results during water leaching for different sulfated samples.

Acid/Red Mud Weight Ratio	0.5	1	1.5	2
Weight loss (%)	47.6	83.28	90.45	97.73

The remaining solids after water leaching were analyzed by XRD. Figure 3c shows the XRD patterns of solid residues for the different samples. For the sample with the lowest acid ratio of 0.5, the main phases identified in the remaining solids were Hematite, Gibbsite, and an aluminosilicate compound known as Epistilbite. Epistilbite was not previously detected, likely due to its low concentration (Figure 3b). Similar compounds were present in the solid residue of the sample with an acid/red mud weight ratio of 1. It is important to

note that the solid residues differ in both phase type and the quantity of remaining solids. While the phase types are similar for the samples with ratios of 0.5 and 1, the amount of insoluble compounds is significantly higher in the sample with the lower ratio compared to the sample with a ratio of 1 (Figure 3c and Table 4).

Phase detection was somewhat challenging for the sample with a ratio of 1.5 due to a noisy diffraction pattern. Nonetheless, several phases of oxides, oxide sulfates, silicates, and sulfates for aluminum, calcium, and iron were identified (Figure 3c). For the sample with the highest acid/red mud weight ratio of 2, similar phases were detected as in the sample with a ratio of 1.5. It should also be noted that the amount of undissolved aluminum and iron oxide sulfates was very low in the residues from ratios of 1.5 and 2. This is attributed to the substantial weight loss during water leaching (Table 4) and the presence of other insoluble compounds.

3.5. Thermal Analysis by TGA-DTA

Figure 3d,e present the TGA-DTA analysis results for both the initial red mud sample and the sulfated sample (with an acid/red mud ratio of 2). As shown in Figure 3d, the red mud exhibited approximately 1% weight loss below 250 °C, which corresponded to its moisture content, indicating that drying occurs within this temperature range. The subsequent weight loss of about 12% below 800 °C was likely due to the elimination of chemically bound water and/or some organic substances. The final weight loss stage is attributed to the calcination of calcium carbonate.

For the sulfated sample, the weight loss observed below 300 °C is attributed to the removal of water and residual sulfuric acid (Figure 3e). The gradual weight loss between 400 and 600 °C was likely due to the decomposition of titanium sulfate, as indicated by its lowest decomposition temperature (see Table 3). The significant weight loss between 600 and 750 °C, coupled with an exothermic peak in the DTA analysis, is attributed to the thermal decomposition of aluminum and iron sulfates, which are major components of red mud.

It is important to note that the values reported in the literature (Table 3) represent the starting temperatures of decomposition. The actual decomposition occurs over a range of temperatures during heating. Additionally, the complexity of the compounds in the sulfated red mud, as discussed in Figure 3b, contributes to variations in the observed decomposition temperatures, because these compounds are not pure stoichiometric sulfates.

3.6. Phase Analysis of the Roasted Samples

Determining precise decomposition temperatures is more challenging with complex mixtures compared to pure single sulfates due to the intricate nature of the mixture and uncertainties surrounding the decomposition temperatures of rare earth element (REE) sulfates. Based on the thermodynamic evaluation and TGA-DTA results for the sulfated sample, roasting temperatures of 675 °C and 725 °C were selected for the decomposition process.

X-ray diffraction patterns of the roasted sulfated samples with acid/red mud weight ratios of 0.5, 1, 1.5, and 2 are shown in Figure 4. The roasted sample with an acid/red mud weight ratio of 0.5 contained Anhydrite and a hydrated Hematite phase at both 675 °C and 725 °C. Increasing the temperature did not significantly alter the phase structure of the roasted sample (Figure 4a). For samples with higher acid ratios (1.5 and 2), Millosevichite, an aluminum oxide sulfate, was detected alongside dehydrated Hematite and Anhydrite at 675 °C. At the higher roasting temperature of 725 °C, Millosevichite decomposed to Alunogen, another aluminum oxide sulfate with a higher oxygen/aluminum ratio, indicating progress in sulfate dissociation. Additionally, the intensity of Hematite and Anhydrite peaks increased, likely due to further formation of Hematite and a higher degree of crystallization at the higher temperature (Figure 4b).

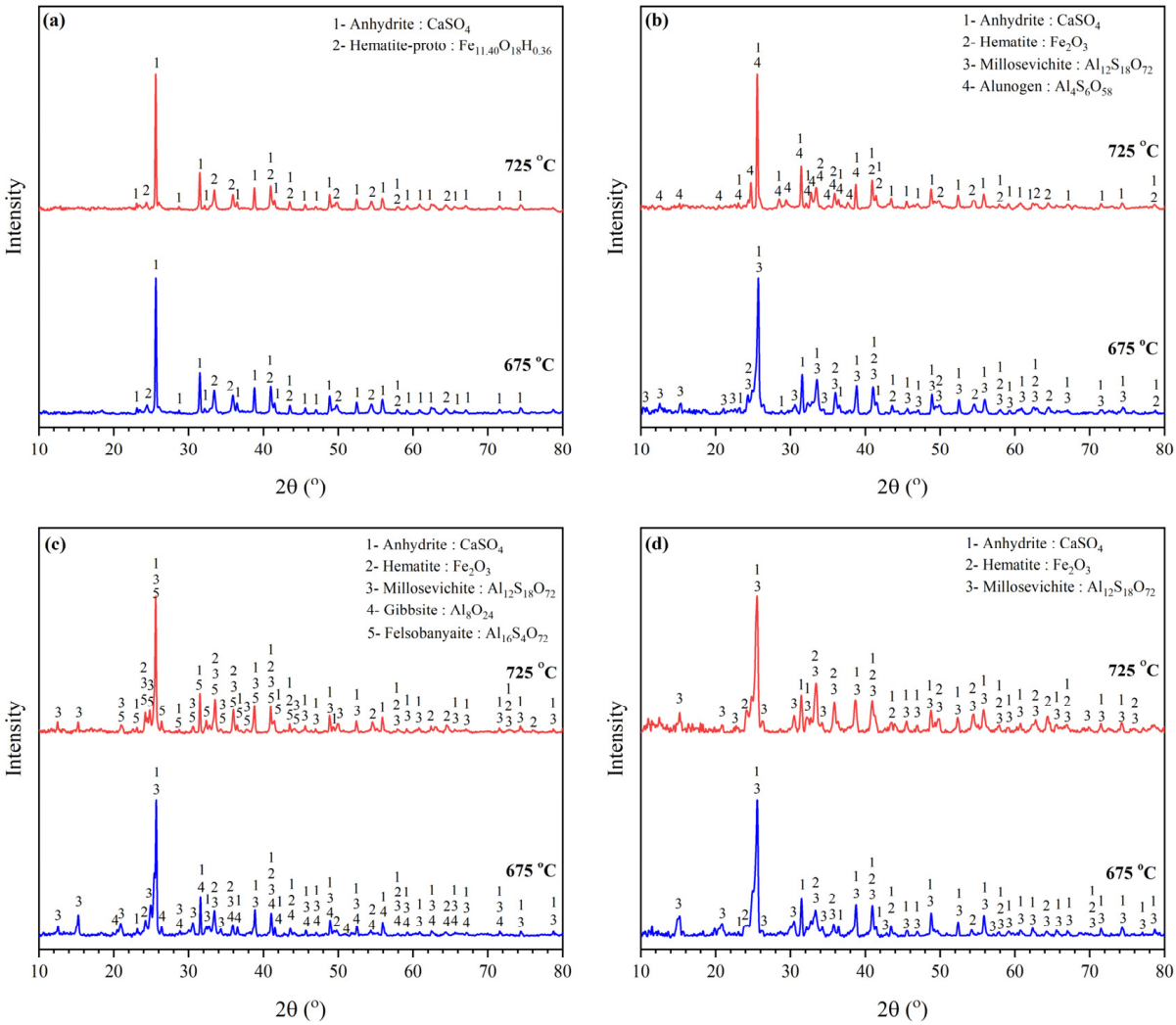

Figure 4. XRD pattern of the roasted samples after sulfation at different acid/red mud weight ratios: (**a**) 0.5, (**b**) 1, (**c**) 1.5, (**d**) 2.

For the sample with an acid/red mud weight ratio of 1.5, Felsobanyatite decomposed into Millosevichite and Gibbsite during roasting at 675 °C (Figures 3b and 4c). Increasing the temperature resulted in the coexistence of Felsobanyatite and Millosevichite. Gibbsite was not detected in the roasted sample at 725 °C, despite the similarities between the two patterns.

In the pattern for the sulfated sample with an acid/red mud weight ratio of 2, Felsobanyatite decomposed into Millosevichite. Additionally, the decomposition of Hohmannite into Hematite during roasting at 675 °C was observed (Figures 3b and 4d). No significant changes in phase composition occured at the higher roasting temperature of 725 °C; however, a slight increase in peak intensity for all three main phases suggested greater stability of the crystalline phases at this temperature. It is worth noting that no traces of titanium oxide or sulfate compounds were observed in any of the patterns, likely due to their low concentration and the formation of partial phases undetectable by XRD.

3.7. Water Leaching

Water leaching experiments were conducted to assess the recovery efficiency of REE sulfates under various conditions. A sulfated sample with an acid/red mud weight ratio of 2 was selected due to the complete sulfation of all elements (Table 4). This sulfated sample, along with the corresponding roasted samples at 675 °C and 725 °C, underwent water

leaching for 1 h with a pulp density of 2% wt./v. The results are shown in Figure 5. For the sulfated sample, over 80% of REEs and undesirable impurities such as Ca, Fe, Al, and Ti were dissolved. In contrast, the dissolution behavior of REEs and impurities varied for the roasted samples. Figure 5a illustrates that yttrium sulfate remained stable up to 675 °C, with about 20% of the sulfate undergoing thermal dissociation and forming water-insoluble yttrium oxide at 725 °C. Dysprosium sulfate behaved similarly, with around 84% remaining stable at 675 °C and about 30% dissociation occurring at 725 °C. Europium sulfate exhibited a different pattern, with 37% dissociation at 675 °C, remaining constant up to 725 °C. Lanthanum and cerium sulfates showed a consistent trend, with approximately 16% and 17% thermal dissociation, respectively, at each temperature increment. Consequently, around 60% of La and Ce could be recovered by water leaching even after roasting at 725 °C, allowing separation from most sulfate impurities with lower thermal stability. The dissolution efficiency of Y, Dy, La, and Ce was approximately 10% lower than in a comparable study and showed greater sensitivity to the roasting temperature [43]. For Tb, Nd, and Gd sulfates, roasting led to about 20% remaining soluble sulfates after 2 h at 725 °C. Thus, roasting for these REEs starts below 675 °C but progresses at different rates up to the maximum applied temperature. Y and Dy exhibited a slower initial rate, increasing with temperature, while La and Ce sulfates dissociated at a relatively constant low rate, and Eu, Tb, Nd, and Gd sulfates converted to oxides more rapidly. The experimental results differed somewhat from the theoretical and experimental onset temperatures reported in Table 3, particularly for Eu, Tb, Nd, Gd, and La. Yttrium sulfate's onset temperature aligned well with the theoretical value. Ce and Dy sulfates' onset temperatures were closer to the experimental and theoretical values, respectively. Differences in thermal dissociation behavior may be attributed to the impurities in the sulfates, as the compounds in this study were not pure and may have interacted with each other, affecting their thermodynamic properties. The values in Table 3 are reported for pure compounds with an activity of 1, while the compounds in the sulfated sample are not pure sulfates, allowing for the possibility of solubilization among different sulfates. Consequently, the impurities in the sulfates could have led to variations in thermodynamic properties, including thermal dissociation temperature.

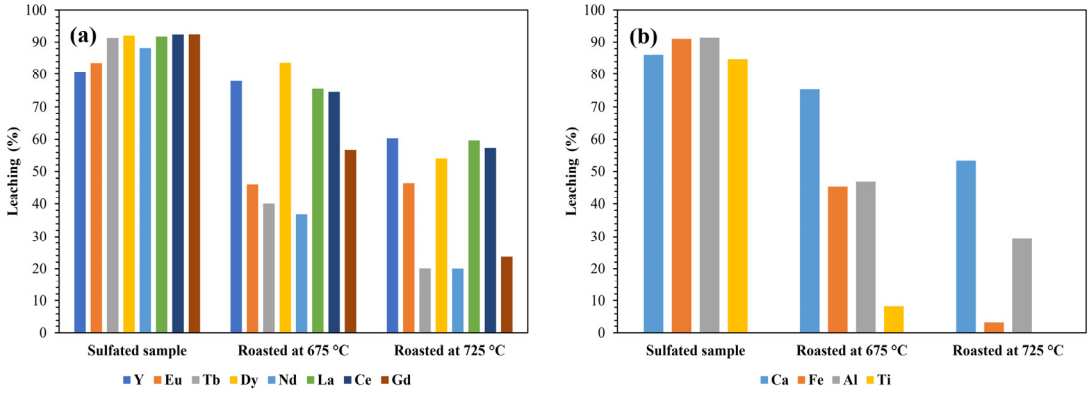

Figure 5. Water leaching results for (**a**) REEs and (**b**) undesirable elements in different samples.

Figure 5b shows the water leaching results for undesirable elements Ca, Fe, Al, and Ti. These results are consistent with Figure 4d, which demonstrates a reduction in the amount of soluble sulfates and an increase in the quantity of insoluble oxides at higher roasting temperatures. Calcium sulfate remained stable due to its high thermal stability, resulting in similar Ca concentration in the solution for both sulfated and roasted samples. However, a decreasing leaching efficiency trend for calcium was observed with increasing roasting temperature, attributed to the enrichment of Ca in the solids caused by weight loss during roasting. Chemical analysis shows a Ca content of approximately 4.7%, 7.5%, and 10% for the sulfated sample and roasted samples at 675 °C and 725 °C, respectively. This corresponds to about 0.1 g Ca per 100 mL of water for all samples, considering a constant

pulp density of 2% wt./v. Iron sulfate began to dissociate below 675 °C, with approximately 46% converted to Hematite at this temperature, which aligns with the experimental onset temperatures in Table 3. Nearly complete conversion of sulfate to oxide was observed at 725 °C, with only 3% residual iron sulfate. Aluminum sulfate roasting behavior was similar to iron sulfate, beginning below 675 °C, but with slower progress, resulting in 30% residual sulfate at 725 °C. Titanium sulfate roasting was faster, reaching nearly complete conversion at 675 °C, with only about 8% residual sulfate. Titanium sulfate was fully converted to oxide at 725 °C. It should be mentioned that the dissolution efficiency of Fe and Ti was similar to that in the comparable study, while the dissolution of Al was higher [43].

3.8. Citric Acid Leaching

This section examines the citric acid leaching of the initial red mud and sulfated samples roasted at 675 °C and 725 °C. Leaching experiments were conducted using a 0.5 M citric acid solution, with a pulp density of 5% wt./v, at 80 °C for up to 6 h. The results are presented in Figure 6.

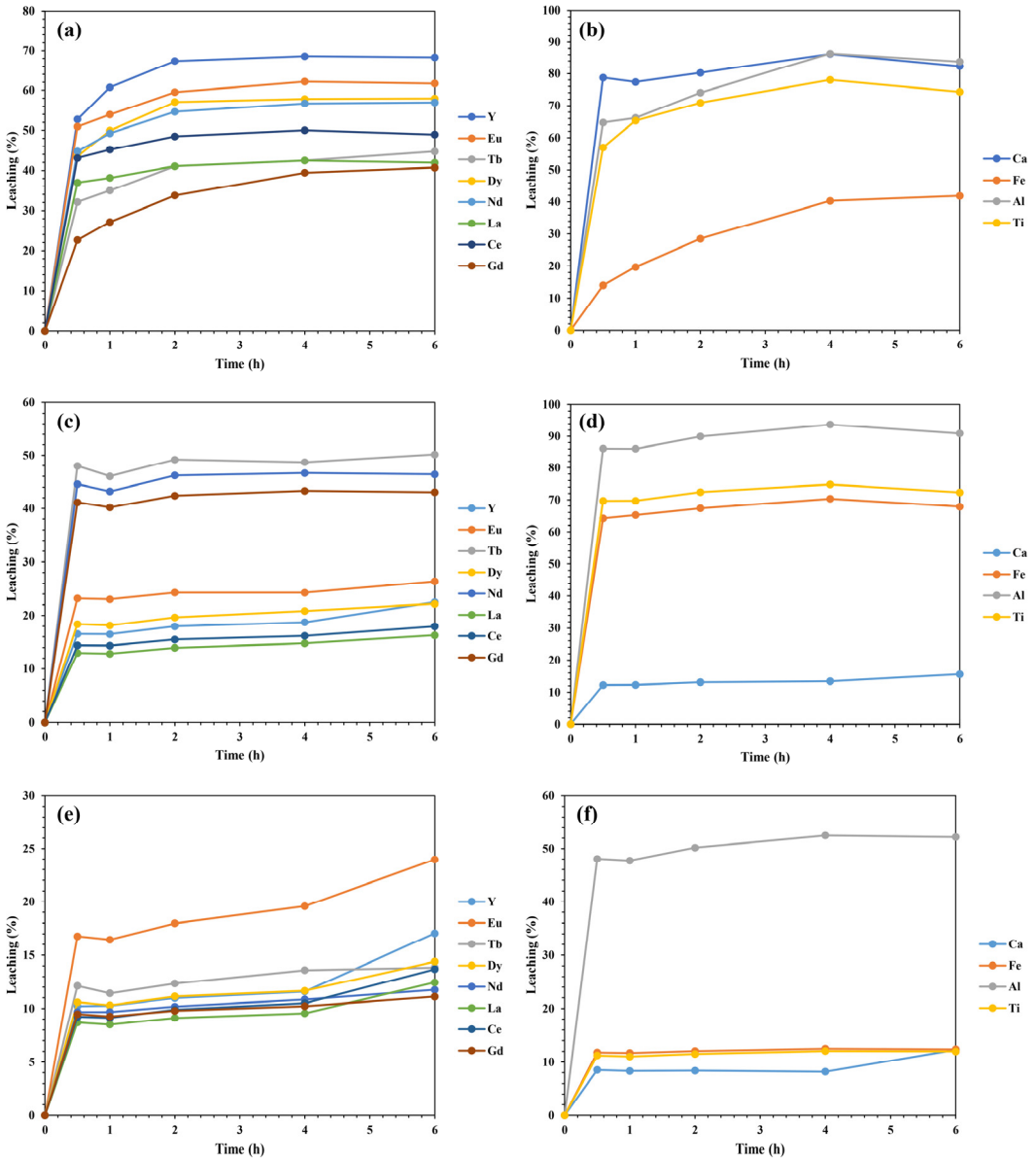

Figure 6. Citric acid leaching results of REEs and undesirable elements for red mud (**a**,**b**), roasted sample at 675 °C (**c**,**d**), and roasted sample at 725 °C (**e**,**f**). Leaching conditions: 0.5 M citric acid at 80 °C and 5% wt./v of pulp density.

Figure 6a shows the leaching efficiency of REEs from the red mud sample. The leaching efficiency increased up until two hours of leaching and then leveled off for most REEs, with the exception of gadolinium. Yttrium exhibited the highest leaching efficiency, reaching a maximum of 68% after 6 h, while gadolinium showed the lowest, with a maximum of 40%. Among the undesirable elements, more than 65% of Ca, Al, and Ti were dissolved after 1 h, while only about 20% of Fe was leached during the same period. Figure 6b indicates that iron was dissolved at the lowest rate, with a maximum of 41% after 6 h. To achieve a high leaching efficiency for REEs and low concentration of undesirable elements in the solution, a leaching time of 1 h is optimal (Figure 6a,b). A comparison with a similar study after 24 h of leaching shows that the leaching efficiency of REEs in citric acid was higher in this study, while the leaching efficiency of Fe was lower than in the comparable study [46].

Figure 6c,d present the leaching results for the sulfated sample roasted at 675 °C. The leaching efficiency for most REEs, except for Gd and Tb, decreased compared to the red mud sample. This reduction suggests that the roasting process converts primary REE minerals into more refractory compounds with lower solubility in citric acid (Figure 6c). In other words, the REE cations were rearranged into the crystal structure of newly formed compounds after the sulfation roasting process. The leaching efficiency for iron increased due to the presence of residual iron sulfate after roasting at 675 °C, while Ca dissolution decreased due to the formation of calcium sulfate (Figure 6d).

Increasing the roasting temperature to 725 °C further decreased the leaching efficiency of REEs, likely due to the completion of the rearrangement process of REE cations into the structure of more refractory compounds (Figure 6e). As anticipated, the leaching efficiency of undesirable elements also decreased with higher roasting temperatures and a greater conversion of sulfates to oxides (Figure 6f).

3.9. Solvent Extraction

The leaching solution using citric acid with the highest content of REEs and undesirable elements after 6 h was subjected to solvent extraction experiments. The goal was to investigate the separation behavior of REEs from undesirable elements. DEHPA was used as an extractant and n-Heptane as a diluent. The effects of the two parameters, n-Heptane:DEHPA ratio and mixing time, were evaluated on extraction efficiency, with an organic/aqueous ratio of 1.

Figure 7a,c show an increase in the extraction efficiency of REEs when the n-Heptane:DEHPA ratio increased, while the effect of mixing time was less significant compared to the diluent/extractant ratio. Notably, more than 80% of REEs, except terbium and neodymium, were extracted at an n-Heptane ratio of 50:50 after 15 and 30 min.

Figure 7b,d illustrate that the extraction efficiency for undesirable elements, excluding calcium, increased significantly with both a higher n-Heptane:DEHPA ratio and longer mixing time. Almost all iron, aluminum, and titanium were extracted at an n-Heptane:DEHPA ratio of 50:50 (Figure 7b). In contrast, less than 24% of these elements were co-extracted into the organic phase at a n-Heptane:DEHPA ratio of 90:10 after 15 min of mixing (Figure 7d). Therefore, the extraction efficiency of undesirable elements was more sensitive to the concentration of the extractant in the organic phase compared to the REEs. Hence, optimization of this parameter is of great importance for practical applications.

Solvent extraction was also applied to the leaching solution obtained from the water leaching of the roasted sample at 725 °C. This solution contained lower levels of Ca, Fe, and Al, with no Ti present (Figure 5b). Figure 7e,f show the extraction efficiency of REEs and undesirable elements at an n-Heptane:DEHPA ratio of 90:10 after 15 min of mixing. The extraction efficiency of REEs was high, including for Tb and Nd. Concurrently, the extraction percentages of Ca, Fe, and Al were higher compared to the citric acid leaching solution (Figure 7b,d). It should be noted that only 3.4% of iron was dissolved in water (Figure 5b), which resulted in a lower Fe concentration in the final solution, despite 60% extraction into the organic phase. Thus, the final solution was expected to have a lower content of undesirable elements.

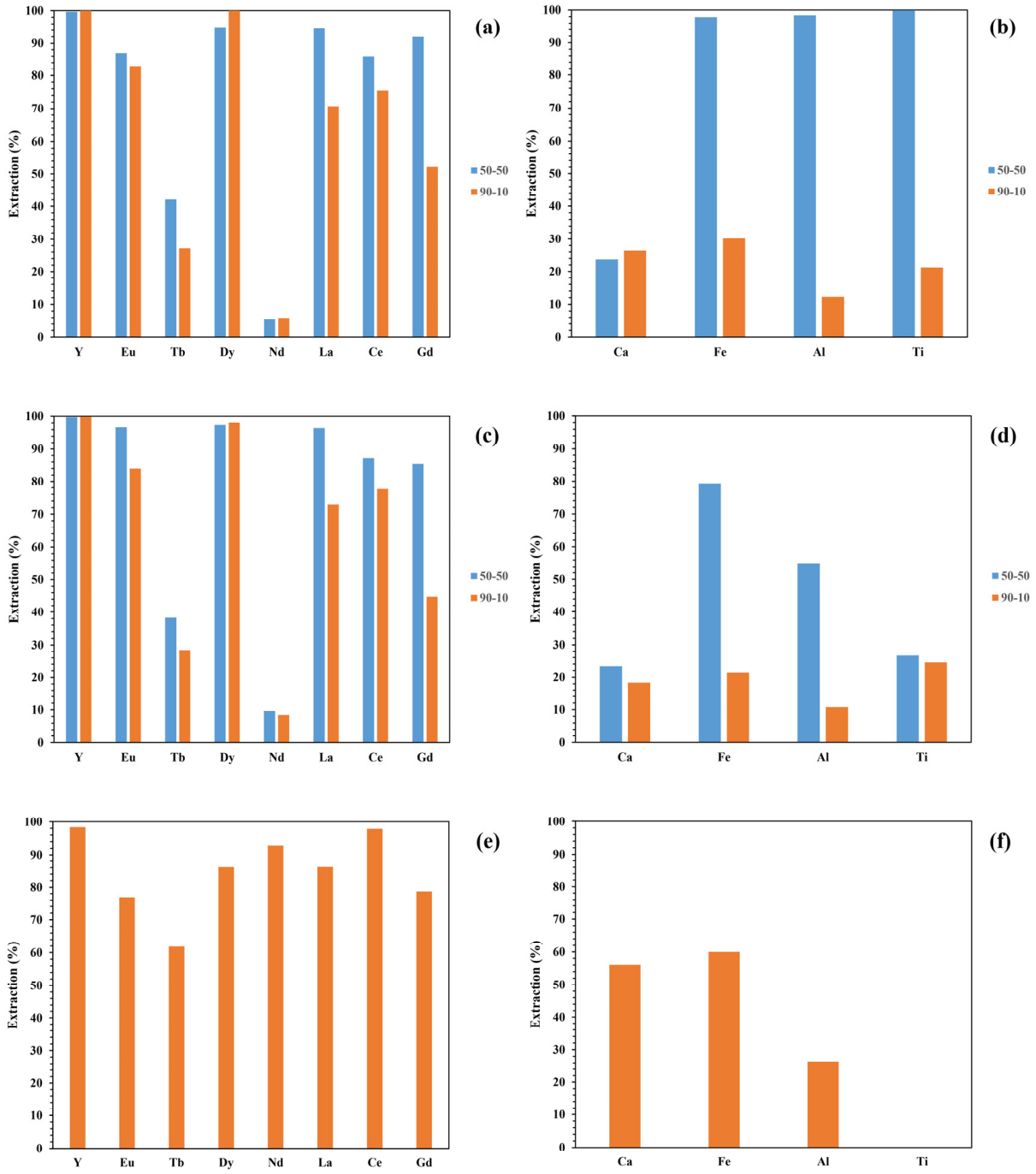

Figure 7. (**a**–**d**) Extracted values of REEs and undesirable elements from citric acid leaching solution of red mud into organic phase for different n-Heptane:DEHPA ratios: (**a**,**b**) 30 min of mixing, (**c**,**d**) 15 min of mixing. (**e**,**f**) Extracted values of REEs (**e**), and undesirable elements (**f**) from water leaching solution of roasted sample at 725 °C into organic phase at n-Heptane:DEHPA ratio of 90:10 and mixing duration of 15 min. A/O ratio was equal to 1 for all experiments.

Stripping experiments were conducted to recover elements of interest from the organic phase into an aqueous solution. The organic phase, loaded with elements from the citric acid leaching solution and using an n-Heptane:DEHPA ratio of 90:10, after 15 min of mixing, was subjected to stripping. Sulfuric acid was chosen as the stripping agent, and its concentration was evaluated for its effect on stripping efficiency. The loaded organic phase and sulfuric acid solution were mixed for 30 min. Figure 8a illustrates that a 6M sulfuric acid solution effectively stripped most REEs, with approximately 50% of terbium

also being recovered. In contrast, lower concentrations of sulfuric acid resulted in lower stripping efficiencies, particularly for yttrium and dysprosium. Figure 8b shows that increasing the sulfuric acid concentration inversely affected the stripping of calcium, while only minimal amounts of iron, aluminum, and titanium were stripped across all tested acid concentrations. Thus, a 6M sulfuric acid solution was deemed effective for stripping the organic phase loaded with the citric acid-pregnant leaching solution.

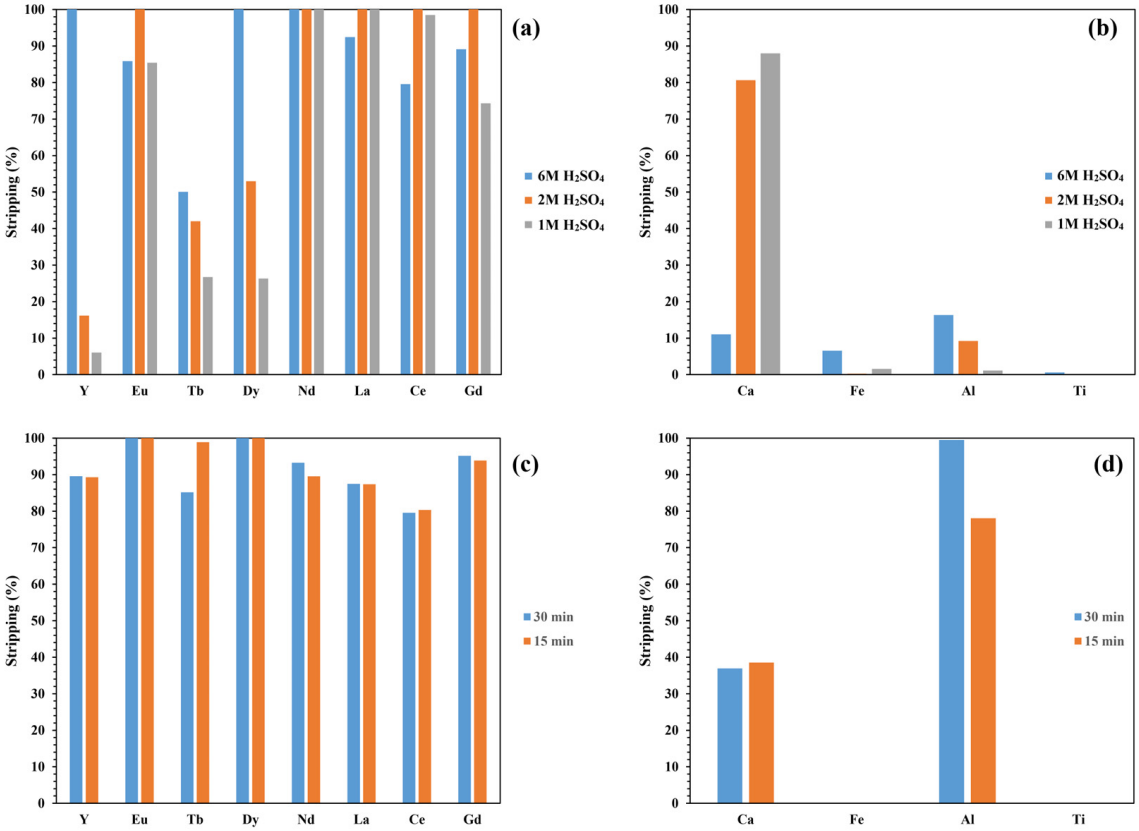

Figure 8. (**a**,**b**): Stripped values of REEs (**a**) and undesirable elements (**b**) after 30 min, at different sulfuric acid concentrations, from citric acid leaching of red mud, extracted at n-Heptane:DEHPA ratio of 90:10, with mixing duration of 15 min. (**c**,**d**): Stripped values of REEs (**c**) and undesirable elements (**d**), using a 6M sulfuric acid solution at different mixing durations, from water leaching of sulfated sample at 725 °C, extracted at n-Heptane:DEHPA ratio of 90:10, with mixing duration of 15 min. A/O ratio was equal to 1 for all experiments.

The loaded organic phase from the water leaching of the roasted sample at 725 °C was also subjected to stripping with 6M sulfuric acid solution, evaluated over different mixing durations (Figure 8c,d). More than 80% of all REEs were stripped after 15 and 30 min, with no significant difference in stripping efficiency between the two durations (Figure 8c). Concurrently, 38% of Ca, 78% of Al, and none of the Fe were stripped after 15 min of mixing (Figure 8d). Mixing duration significantly impacted aluminum stripping, with complete recovery achieved after 30 min, while the stripping efficiency of Ca remained constant.

3.10. Concluding Remarks

In this research, two methods were investigated for recovering REEs from red mud. The sulfation roasting–water leaching process revealed that even at roasting temperatures as high as 725 °C, approximately 3.4% of iron and 29.6% of aluminum remained as soluble sulfates, leading to their presence as undesirable elements in the water leaching solution. A positive aspect of this process was the complete removal of titanium at 725 °C. However, the high dissolved value of calcium could be significantly reduced by employing higher pulp

densities during leaching or by recirculating the leaching solution using a cross-leaching process, given the limited solubility of calcium sulfate in water.

Increasing the roasting temperature also decreases REEs dissolution. Therefore, while reducing impurity content in the solution by raising the roasting temperature, this approach resulted in lower REE recovery rates. On the other hand, the results indicated that solvent extraction could reduce impurity content to some extent. Consequently, we suggest combining the sulfation roasting–water leaching process with solvent extraction to enhance the separation efficiency of REEs from undesirable elements. The study showed that this combined approach yields a final solution containing 2 mg/L of REEs and 132 mg/L of undesirable elements, with about 80% of the impurity content being Ca. This calcium content can be significantly reduced by increasing the pulp density or recirculating the water leaching solution for a new leaching step of the roasted sample. A scheme of the proposed process is shown in Figure 9a.

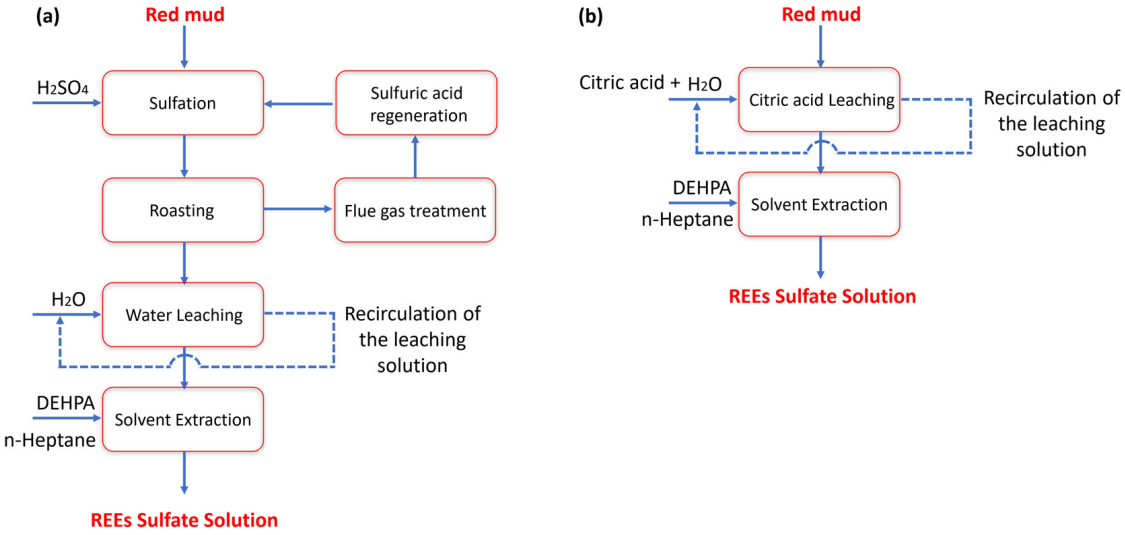

Figure 9. (**a**) A scheme of the proposed Sulfation roasting–Water leaching–Solvent extraction process, (**b**) A scheme of the proposed Citric acid leaching–Solvent extraction process.

In the citric acid leaching process, 40%–60% of REEs were dissolved in a 0.5M citric acid solution at 80 °C over a period of 6 h. A drawback of this method is the higher leaching rate of undesirable elements compared to the sulfation roasting–water leaching process. However, fewer impurities were co-extracted and stripped during the solvent extraction stage. The results showed that this process yielded a final solution containing 9.75 mg/L of REEs and 207 mg/L of undesirable elements. It's important to note that a higher pulp density was used in this process compared to the sulfation roasting–water leaching process (5% wt./v versus 1% wt./v). A scheme of the proposed process is shown in Figure 9b.

The combination of the two processes, sulfation roasting plus citric acid leaching, was found to be inefficient, as the citric acid leaching efficiency of the roasted samples decreased with increasing roasting temperature. This decrease is likely due to the phase differences and complexities between the primary red mud and the mineralized compounds formed in the roasted samples (Figures 3 and 4).

Finally, the advantages and disadvantages of the two processes are summarized in Table 5. Based on the results, citric acid leaching followed by solvent extraction appears to be a better choice than the sulfation roasting–water leaching-solvent extraction process. It is evident that REE concentration can be improved by increasing pulp density and by recirculating the solution using a cross-leaching method, which can be optimized in future studies.

Table 5. Advantages and disadvantages of two investigated processes.

Process	Advantages	Disadvantages
Sulfation roasting–Water leaching–Solvent extraction	• Capable of removing most of Ti and Fe during the roasting process • Uses water as the leaching agent • Ability to regenerate sulfuric acid • Simple process	• Complex process • High energy consumption • Special need for flue gas treatment (SO_3)
Citric acid leaching–Solvent extraction	• Green process due to biodegradability of wastewater for treatment • No need for flue gas treatment • Lower energy consumption • Relatively higher leaching efficiency of REEs	• Higher leaching rate of undesirable elements

4. Conclusions

1- XRD investigations revealed that the primary complex oxide and silicate compounds in red mud are converted mostly to sulfates during the sulfation process, in an acid/red mud weight ratio of 2, which are converted subsequently to oxide and oxide sulfate compounds in the roasting process.

2- Increasing roasting temperature to 725 °C can reduce the water leaching efficiency of Ti and Fe significantly, but about 30% of Al remained water soluble. Increasing the temperature is not suggested, due to the decrease of the leaching efficiency of REEs.

3- The citric acid leaching of red mud led to a higher leaching efficiency of REEs and undesirable elements, in comparison with the sulfation roasting–water leaching process. On the other hand, the citric acid leaching of the roasted sample at 725 °C resulted in a lower leaching efficiency of REEs and undesirable elements.

4- The solvent extraction experiments illustrated that in the citric acid leaching process, the extraction efficiency of undesirable elements is more sensitive to both the concentration of extractant in the organic phase and mixing time than the REEs. The results also showed that the extraction efficiency of REEs and undesirable elements in the pregnant leaching solution of water leaching is higher than in the citric acid leaching solution.

5- The stripping experiments revealed that sulfuric acid concentration has a significant effect on the recovery of Y, Tb, Dy, and Ca from citric acid solution. About 50% of Tb and more than 80% of other REEs were stripped using a 6M H_2SO_4 solution, while about 11%, 6.5%, and 16% of Ca, Fe, and Al were stripped, respectively, at the same time.

6- The same stripping conditions applied to the water leaching solution illustrated that more than 80% of REEs, except for Tb, were stripped in 15 min using 6M sulfuric acid solution, with the same results after 30 min. Regarding the impurity elements, only Ca and Al were stripped in such conditions, with higher Al stripping efficiency after 30 min of mixing.

Author Contributions: Conceptualization, H.S. and F.V.; methodology, H.S.; software, H.S.; validation, H.S., A.B. and F.V.; formal analysis, H.S. and F.V.; investigation, H.S. and M.H.N.; resources, A.B. and F.V.; data curation, H.S. and A.B.; writing—original draft preparation, H.S.; writing—review and editing, F.V., I.B. and A.B; visualization, H.S. and A.B.; supervision, F.V. and A.B.; project administration, A.B.; funding acquisition, A.B. and F.V. All authors have read and agreed to the published version of the manuscript.

Funding: This research received no external funding.

Data Availability Statement: Data are contained within the article.

Acknowledgments: The authors thank the Iran Alumina Company for providing red mud sample.

Conflicts of Interest: The authors declare no conflicts of interest.

References

1. Agrawal, S.; Dhawan, N. Evaluation of red mud as a polymetallic source—A review. *Miner. Eng.* **2021**, *171*, 107084. [CrossRef]
2. Wang, M.; Liu, X. Applications of red mud as an environmental remediation material: A review. *J. Hazard. Mater.* **2021**, *408*, 124420. [CrossRef] [PubMed]
3. Wang, S.; Jin, H.; Deng, Y.; Xiao, Y. Comprehensive utilization status of red mud in China: A critical review. *J. Clean. Prod.* **2021**, *289*, 125136. [CrossRef]
4. Agrawal, S.; Rayapudi, V.; Dhawan, N. Comparison of microwave and conventional carbothermal reduction of red mud for recovery of iron values. *Miner. Eng.* **2019**, *132*, 202–210. [CrossRef]
5. Rai, S.; Bahadure, S.; Chaddha, M.; Agnihotri, A. Disposal practices and utilization of red mud (Bauxite Residue): A review in Indian context and abroad. *J. Sustain. Metall.* **2020**, *6*, 1–8. [CrossRef]
6. Power, G.; Gräfe, M.; Klauber, C. Bauxite residue issues: I. Current management, disposal and storage practices. *Hydrometallurgy* **2011**, *108*, 33–45. [CrossRef]
7. Zhou, G.-T.; Wang, Y.-L.; Qi, T.-G.; Zhou, Q.-S.; Liu, G.-H.; Peng, Z.-H.; Li, X.-B. Toward sustainable green alumina production: A critical review on process discharge reduction from gibbsitic bauxite and large-scale applications of red mud. *J. Environ. Chem. Eng.* **2023**, *11*, 109433. [CrossRef]
8. Li, X.-F.; Zhang, T.-A.; Lv, G.-Z.; Wang, K.; Wang, S. Summary of Research Progress on Metallurgical Utilization Technology of Red Mud. *Minerals* **2023**, *13*, 737. [CrossRef]
9. Shengguo, X.; Yubing, L.; Ying, G. Environmental impact of bauxite residue: A comprehensive review. *J. Univ. Chin. Acad. Sci.* **2017**, *34*, 401.
10. Lu, G.-Z.; Zhang, T.-A.; Ma, L.-N.; Wang, Y.-X.; Zhang, W.-G.; Zhang, Z.-M.; Wang, L. Utilization of Bayer red mud by a calcification—Carbonation method using calcium aluminate hydrate as a calcium source. *Hydrometallurgy* **2019**, *188*, 248–255. [CrossRef]
11. Du, P.; Wang, P.; Zhang, X.; Wen, G.; Wang, Y. Properties, hazards and valuable metal recovery technologies of red mud: A review. *Particuology* **2024**, *93*, 328–348. [CrossRef]
12. Wang, L.; Sun, N.; Tang, H.; Sun, W. A review on comprehensive utilization of red mud and prospect analysis. *Minerals* **2019**, *9*, 362. [CrossRef]
13. Loganathan, P.; Vigneswaran, S.; Kandasamy, J.; Bolan, N.S. Removal and recovery of phosphate from water using sorption. *Crit. Rev. Environ. Sci. Technol.* **2014**, *44*, 847–907. [CrossRef]
14. Kazak, O.; Tor, A. In situ preparation of magnetic hydrochar by co-hydrothermal treatment of waste vinasse with red mud and its adsorption property for Pb (II) in aqueous solution. *J. Hazard. Mater.* **2020**, *393*, 122391. [CrossRef]
15. Qi, X.; Wang, H.; Zhang, L.; Xu, B.; Shi, Q.; Li, F. Removal of Cr (III) from aqueous solution by using bauxite residue (red mud): Identification of active components and column tests. *Chemosphere* **2020**, *245*, 125560. [CrossRef]
16. Shi, W.; Ren, H.; Huang, X.; Li, M.; Tang, Y.; Guo, F. Low cost red mud modified graphitic carbon nitride for the removal of organic pollutants in wastewater by the synergistic effect of adsorption and photocatalysis. *Sep. Purif. Technol.* **2020**, *237*, 116477. [CrossRef]
17. Nie, Q.; Hu, W.; Huang, B.; Shu, X.; He, Q. Synergistic utilization of red mud for flue-gas desulfurization and fly ash-based geopolymer preparation. *J. Hazard. Mater.* **2019**, *369*, 503–511. [CrossRef]
18. Li, B.; Wu, H.; Liu, X.; Zhu, T.; Liu, F.; Zhao, X. Simultaneous removal of SO_2 and NO using a novel method with red mud as absorbent combined with O3 oxidation. *J. Hazard. Mater.* **2020**, *392*, 122270. [CrossRef]
19. Cheng, L.; Wu, Z.; Zhang, Z.; Guo, C.; Ellis, N.; Bi, X.; Watkinson, A.P.; Grace, J.R. Tar elimination from biomass gasification syngas with bauxite residue derived catalysts and gasification char. *Appl. Energy* **2020**, *258*, 114088. [CrossRef]
20. Krivenko, P.; Kovalchuk, O.; Pasko, A.; Croymans, T.; Hult, M.; Lutter, G.; Vandevenne, N.; Schreurs, S.; Schroeyers, W. Development of alkali activated cements and concrete mixture design with high volumes of red mud. *Constr. Build. Mater.* **2017**, *151*, 819–826. [CrossRef]
21. Tang, W.; Wang, Z.; Donne, S.; Forghani, M.; Liu, Y. Influence of red mud on mechanical and durability performance of self-compacting concrete. *J. Hazard. Mater.* **2019**, *379*, 120802. [CrossRef]
22. Liu, R.-X.; Poon, C.-S. Utilization of red mud derived from bauxite in self-compacting concrete. *J. Clean. Prod.* **2016**, *112*, 384–391. [CrossRef]
23. Kim, Y.; Kim, M.; Sohn, J.; Park, H. Applicability of gold tailings, waste limestone, red mud, and ferronickel slag for producing glass fibers. *J. Clean. Prod.* **2018**, *203*, 957–965. [CrossRef]
24. Zhao, J.; Wang, Y.; Kang, J.; Qu, Y.; Khater, G.; Li, S.; Shi, Q.; Yue, Y. Effect of SnO2 on the structure and chemical durability of the glass prepared by red mud. *J. Non-Cryst. Solids* **2019**, *509*, 54–59. [CrossRef]
25. Jahromi, H.; Agblevor, F.A. Hydrodeoxygenation of aqueous-phase catalytic pyrolysis oil to liquid hydrocarbons using multifunctional nickel catalyst. *Ind. Eng. Chem. Res.* **2018**, *57*, 13257–13268. [CrossRef]
26. Das, B.; Mohanty, K. A green and facile production of catalysts from waste red mud for the one-pot synthesis of glycerol carbonate from glycerol. *J. Environ. Chem. Eng.* **2019**, *7*, 102888. [CrossRef]

27. Shim, W.G.; Nah, J.W.; Jung, H.-Y.; Park, Y.-K.; Jung, S.C.; Kim, S.C. Recycling of red mud as a catalyst for complete oxidation of benzene. *J. Ind. Eng. Chem.* **2018**, *60*, 259–267. [CrossRef]
28. Kurtoğlu, S.F.; Soyer-Uzun, S.; Uzun, A. Utilizing red mud modified by simple treatments as a support to disperse ruthenium provides a high and stable performance for COx-free hydrogen production from ammonia. *Catal. Today* **2020**, *357*, 425–435. [CrossRef]
29. Pan, X.; Wu, H.; Lv, Z.; Yu, H.; Tu, G. Recovery of valuable metals from red mud: A comprehensive review. *Sci. Total Environ.* **2023**, *904*, 166686. [CrossRef]
30. Yuan, S.; Liu, X.; Gao, P.; Han, Y. A semi-industrial experiment of suspension magnetization roasting technology for separation of iron minerals from red mud. *J. Hazard. Mater.* **2020**, *394*, 122579. [CrossRef]
31. Li, S.; Kang, Z.; Liu, W.; Lian, Y.; Yang, H. Reduction behavior and direct reduction kinetics of red mud-biomass composite pellets. *J. Sustain. Metall.* **2021**, *7*, 126–135. [CrossRef]
32. Wei, D.; Jun-Hui, X.; Yang, P.; Si-Yue, S.; Tao, C. Iron extraction from red mud using roasting with sodium salt. *Miner. Process. Extr. Metall. Rev.* **2021**, *42*, 153–161. [CrossRef]
33. Li, R.; Zhang, T.; Liu, Y.; Lv, G.; Xie, L. Calcification–carbonation method for red mud processing. *J. Hazard. Mater.* **2016**, *316*, 94–101. [CrossRef]
34. Agrawal, S.; Dhawan, N. Investigation of mechanical and thermal activation on metal extraction from red mud. *Sustain. Mater. Technol.* **2021**, *27*, e00246. [CrossRef]
35. Zhang, R.; Zheng, S.; Ma, S.; Zhang, Y. Recovery of alumina and alkali in Bayer red mud by the formation of andradite-grossular hydrogarnet in hydrothermal process. *J. Hazard. Mater.* **2011**, *189*, 827–835. [CrossRef]
36. Pepper, R.A.; Couperthwaite, S.J.; Millar, G.J. Comprehensive examination of acid leaching behaviour of mineral phases from red mud: Recovery of Fe, Al, Ti, and Si. *Miner. Eng.* **2016**, *99*, 8–18. [CrossRef]
37. Huang, Y.; Chai, W.; Han, G.; Wang, W.; Yang, S.; Liu, J. A perspective of stepwise utilisation of Bayer red mud: Step two—Extracting and recovering Ti from Ti-enriched tailing with acid leaching and precipitate flotation. *J. Hazard. Mater.* **2016**, *307*, 318–327. [CrossRef] [PubMed]
38. Agatzini-Leonardou, S.; Oustadakis, P.; Tsakiridis, P.; Markopoulos, C. Titanium leaching from red mud by diluted sulfuric acid at atmospheric pressure. *J. Hazard. Mater.* **2008**, *157*, 579–586. [CrossRef]
39. Borra, C.R.; Blanpain, B.; Pontikes, Y.; Binnemans, K.; Van Gerven, T. Smelting of bauxite residue (red mud) in view of iron and selective rare earths recovery. *J. Sustain. Metall.* **2016**, *2*, 28–37. [CrossRef]
40. Reid, S.; Tam, J.; Yang, M.; Azimi, G. Technospheric mining of rare earth elements from bauxite residue (red mud): Process optimization, kinetic investigation, and microwave pretreatment. *Sci. Rep.* **2017**, *7*, 15252. [CrossRef]
41. Narayanan, R.P.; Kazantzis, N.K.; Emmert, M.H. Selective process steps for the recovery of scandium from Jamaican bauxite residue (red mud). *ACS Sustain. Chem. Eng.* **2018**, *6*, 1478–1488. [CrossRef]
42. Borra, C.R.; Blanpain, B.; Pontikes, Y.; Binnemans, K.; Van Gerven, T. Recovery of rare earths and major metals from bauxite residue (red mud) by alkali roasting, smelting, and leaching. *J. Sustain. Metall.* **2017**, *3*, 393–404. [CrossRef]
43. Borra, C.R.; Mermans, J.; Blanpain, B.; Pontikes, Y.; Binnemans, K.; Van Gerven, T. Selective recovery of rare earths from bauxite residue by combination of sulfation, roasting and leaching. *Miner. Eng.* **2016**, *92*, 151–159. [CrossRef]
44. Pasechnik, L.; Skachkov, V.; Chufarov, A.Y.; Suntsov, A.Y.; Yatsenko, S. High purity scandium extraction from red mud by novel simple technology. *Hydrometallurgy* **2021**, *202*, 105597. [CrossRef]
45. Akcil, A.; Swami, K.R.; Gardas, R.L.; Hazrati, E.; Dembele, S. Overview on Hydrometallurgical Recovery of Rare-Earth Metals from Red Mud. *Minerals* **2024**, *14*, 587. [CrossRef]
46. Borra, C.R.; Pontikes, Y.; Binnemans, K.; Van Gerven, T. Leaching of rare earths from bauxite residue (red mud). *Miner. Eng.* **2015**, *76*, 20–27. [CrossRef]
47. Zhang, X.-K.; Zhou, K.-G.; Chen, W.; Lei, Q.-Y.; Huang, Y.; Peng, C.-H. Recovery of iron and rare earth elements from red mud through an acid leaching-stepwise extraction approach. *J. Cent. South Univ.* **2019**, *26*, 458–466. [CrossRef]
48. Onghena, B.; Borra, C.R.; Van Gerven, T.; Binnemans, K. Recovery of scandium from sulfation-roasted leachates of bauxite residue by solvent extraction with the ionic liquid betainium bis (trifluoromethylsulfonyl) imide. *Sep. Purif. Technol.* **2017**, *176*, 208–219. [CrossRef]
49. Habibi, H.; Mokmeli, M.; Shakibania, S.; Pirouzan, D.; Pourkarimi, Z. Separation and recovery of titanium and scandium from the red mud. *Sep. Purif. Technol.* **2023**, *317*, 123882. [CrossRef]
50. Quinn, J.E.; Soldenhoff, K.H.; Stevens, G.W.; Lengkeek, N.A. Solvent extraction of rare earth elements using phosphonic/phosphinic acid mixtures. *Hydrometallurgy* **2015**, *157*, 298–305. [CrossRef]
51. Ochsenkühn-Petropulu, M.; Lyberopulu, T.; Parissakis, G. Selective separation and determination of scandium from yttrium and lanthanides in red mud by a combined ion exchange/solvent extraction method. *Anal. Chim. Acta* **1995**, *315*, 231–237. [CrossRef]
52. Zhu, X.; Li, W.; Tang, S.; Zeng, M.; Bai, P.; Chen, L. Selective recovery of vanadium and scandium by ion exchange with D201 and solvent extraction using P507 from hydrochloric acid leaching solution of red mud. *Chemosphere* **2017**, *175*, 365–372. [CrossRef] [PubMed]
53. Banerjee, R.; Mohanty, A.; Chakravarty, S.; Chakladar, S.; Biswas, P. A single-step process to leach out rare earth elements from coal ash using organic carboxylic acids. *Hydrometallurgy* **2021**, *201*, 105575. [CrossRef]
54. Tagawa, H. Thermal decomposition temperatures of metal sulfates. *Thermochim. Acta* **1984**, *80*, 23–33. [CrossRef]

55. Lemm, J.M. *Handbook on the Physics and Chemistry of Rare Earths*; Elsevier: Amsterdam, The Netherlands, 1987; Volume 9.
56. Stern, K.H. *High Temperature Properties and Thermal Decomposition of Inorganic Salts with Oxyanions*; CRC Press: Boca Raton, FL, USA, 2000.
57. Denisenko, Y.G.; Khritokhin, N.; Andreev, O.; Basova, S.; Sal'nikova, E.; Polkovnikov, A. Thermal decomposition of europium sulfates $Eu_2(SO_4)_3 \cdot 8H_2O$ and $EuSO_4$. *J. Solid State Chem.* **2017**, *255*, 219–224. [CrossRef]
58. Rodrigues, R.V.; Machado, L.; Matos, J.D.R.; Muri, E.J.B.; Marins, A.A.L.; Brito, H.F.D.; Passos, C.A.C. Oxysulfate/oxysulfide of Tb^{3+} obtained by thermal decomposition of terbium sulfate hydrates under different atmospheres. *J. Therm. Anal. Calorim.* **2015**, *122*, 765–773. [CrossRef]
59. Tomaszewicz, E.; Leniec, G.; Kaczmarek, S. Re-investigations of thermal decomposition of gadolinium sulfate octahydrate. *J. Therm. Anal. Calorim.* **2010**, *102*, 875–881. [CrossRef]